Improved electrochemical performance of onion-like carbon coated magnetite nanocapsules as electromagnetic absorptive anode materials for lithium-ion batteries

SCHOLARONE™
Manuscripts

RSC Advances

PAPER

Improved electrochemical performance of onion-like carbon coated magnetite nanocapsules as electromagnetic absorptive anode materials for lithium-ion batteries

Nannan Bi,[a] Xianguo Liu,*[a] Niandu Wu,[a] Caiyun Cui,[a] and Yuping Sun[b]

The synthesis of magnetite (Fe_3O_4)@C nanocapsules with Fe_3O_4 nanoparticles as the core and onion-like carbon as the shell has been reported. The electromagnetic (EM) characteristics and electrochemical performance are studied. The onion-like carbon shell improves dielectric loss and EM matching degree,
10 leading to the enhanced EM properties. The optimal reflection loss (RL) value of Fe_3O_4@C-paraffin composite is -45.9 dB at 16.6 GHz at the thickness of 2.4 mm and the absorption bandwidth of 7.2 GHz (RL exceeding -10 dB) covers the 9.8-17.0 GHz at 3.0 mm. The EM absorption mechanism may be explained by the combination of EM loss model and the quarter-wavelength cancellation condition. The onion-like defective carbon shell not only can accommodate the volume change of Fe_3O_4 nanoparticles
15 but also can prevent the formation of solid electrolyte interface films on surface of nanoparticles, resulting in the remarkable electrochemical performance for lithium ion batteries (LIBs). The Fe_3O_4@C nanocapsules display an attractive cycling performance up to 300 cycles (918 mAh g^{-1} retained at 0.1 Ag^{-1}) and a high initial coulomb efficiency of 85.6%. A capacity of 934 mAh g^{-1} is recoverable after charge/discharge process at high rates. The present work represents Fe_3O_4@C nanocapsules as a new kind
20 of EM absorptive anode materials for LIBs.

1. Introduction

Lithium-ion batteries (LIBs), the commercialized rechargeable batteries, have been under research focus in the past decade due to their extensive applications in mobile electronic
25 devices, e.g. mobile telephone and laptop.[1-5] Current LIBs use graphite anodes in which one unit (six carbon atoms for graphite) can store one or less lithium ion, leading to a limited theoretical capacity of 372 mAh g^{-1}.[1-5] In recent years, serious electromagnetic (EM) interference pollution arising from the
30 rapidly expanding use of communication devices at gigahertz range, such as mobile telephone (0.5-3.5 GHz) and laptop (1.5-3.0 GHz), has attracted considerable attention.[6-10] To simultaneously circumvent the low energy density of graphite and the main EM interference problem from electronics utilized
35 currently, multifunctional materials are highly desired.

As an important binary oxide, magnetite (Fe_3O_4) has attracted considerable attention because of the intriguing chemical, electronic, electrochemical, EM and magnetic properties resulting from the transfer of electrons between Fe^{2+}
40 and Fe^{3+} in the octahedral sites.[1,8,9,11,12] Fe_3O_4 as anode material possesses the theoretical capacity of 924 mAh g^{-1}, while Fe_3O_4 can attenuate EM waves efficiently because of their magnetic and dielectric loss.[2,9] Thus, Fe_3O_4 is a promising candidate material for EM absorptive anode materials in LIBs. The extremely high
45 volume change commonly occurs in Fe_3O_4 during the discharge/charge cycling process, which is the bottleneck for the

commercialization. The pulverization problem can cause a breakdown in electrical contact pathways between Fe_3O_4, leading to rapid capacity fading during charge-discharge cycling.[3] In
50 addition, Fe_3O_4 have main disadvantages such as large density (~ 5 g/cm^3) and narrow absorption bandwidth, which restrict their further application in microwave absorbers.

To overcome the above limitations, the carbonaceous materials are proposed to absorb the volume changes and
55 improve the microwave absorption performance. Carbon is an ideal candidate as composite material due to its main advantages: (i) carbon is stable even at harsh application situations such as acids and alkalis, effectively protecting the core materials against environmental degradation and hindering aggregation of
60 neighboring particles;(ii) as a good electric conductor, carbon can overcome the limitation of insulator coating in applications of biosensor and fuel cell.[13] Nanocapsules are capsules of nanometer size, which are normally composed of a core and a shell that are made of different materials. Among Fe_3O_4/C nanoscale
65 composites, core/shell structured nanocapsules with Fe_3O_4 nanoparticles as the core and onion-like carbon as the shell of nanometer size are of particular interest due to the improved strain accommodation capability and the proper EM matching degree. For example, core/shell-structured NiO/C, Co_3O_4/C, and
70 CuO/C nanocapsules all exhibit markedly enhanced lithium storage performance by virtue of their special structural characteristics.[14-16] Core/shell-structured Ni/C, Fe/C, FeNi/C, and FeCo/C nanocapsules show the excellent EM absorptive abilities

due to the proper EM matching from the special microstructure.[17-19]

However, the effect of the onion-like carbon shell on the EM and electrochemical properties of Fe_3O_4 nanoparticles has not been systematically investigated yet. In the present work, onion-like carbon coated Fe nanocapsules have been prepared by arc discharging a Fe ingot under the alcohol vapor. Onion-like carbon coated Fe_3O_4 nanocapsules and Fe_3O_4 nanoparticles, which have been obtained after the heating treatment of Fe nanocapsules with different temperature in air, are studied in detail, in particular concerning the influence of onion-like carbon shell on the EM and electrochemical properties of Fe_3O_4 nanoparticles.

2. Experimental

2.1 Synthesis of Fe_3O_4@C nanocapsules

Fe@C nanocapsules were prepared by the modified arc-discharge method described in detail elsewhere.[14-19] In brief, bulk Fe on a water-cooled copper crucible was used as the anode. The cathode was a carbon needle. After the chamber was evacuated, 1.6×10^4 Pa of pure argon and 0.4×10^4 Pa of hydrogen and 40 ml liquid ethanol were introduced into the chamber. The arc discharge current was maintained at 100 A for 0.5 h. The partial pressure of ethanol increased with the time. When the arc time reached 0.5 h, the pressure of the chamber can reach 1 atmospheric pressure because of the decomposition of ethanol and the expand of the gas with increasing the temperature. Then the products (sample a) were collected from depositions on the top of the water-cooled chamber, after passivated for 24 h in air. In order to get the enough products for the measurement of microwave absorption characteristics and electrochemical performance, the above experiment was repeated several times under the same experiment conditions. To prepare the carbon-coated Fe_3O_4 nanocapsules (sample b) and Fe_3O_4 nanoparticles (sample c), the products were annealed at 80 and 200 ^{o}C for 1 h in air, respectively.

2.2 Materials characterizations

The composition and phase purity of the as-prepared products were examined by an X-ray diffractometer (XRD, Brucker D8 Advance, Germany) at 40 kV voltage and 50 mA current and with CuK$_\alpha$ radiation (λ=1.5418 Å). The morphologies of the products were captured using a transmission electron microscope (TEM, JEOL-2010F, Japan) at an acceleration voltage of 200 kV.

2.3 Electromagnetic absorbing measurement

Paraffin-bonded Fe_3O_4 nanocapsules/nanoparticles composites were prepared by uniformly mixing 40 wt.% Fe_3O_4 nanocapsules/nanoparticles in the paraffin matrix and by pressing the mixture into cylinder-shaped compacts. More details can be found elsewhere.[17-19] The prepared compacts were cut into toroidal samples with 7.00 mm outer diameter and 3.04 mm inner diameter. The EM parameters of the toroidal samples were evaluated in the frequency range of 2-18 GHz, using a vector network analyzer (Agilent N5244A, USA) in conjunction with a coaxial method in transverse EM mode. The vector network analyzer (VNA) was calibrated for the full two-port measurement of reflection and transmission at each port. The complex permittivity ($\varepsilon_\gamma = \varepsilon' - j\varepsilon''$) and complex permeability ($\mu_\gamma = \mu' - j\mu''$) were calculated from S-parameters tested by the VNA using the simulation program of Reflection/Transmission Nicolson-Ross model.[19]

2.4 Electrochemical tests

Electrochemical experiments were carried out by using standard CR2032 type coin cells. The working electrodes were prepared by mixing the Fe_3O_4 nanocapsules/nanoparticles, carbon black and poly(vinyl difluoride) at weight ratio of 80:10:10 and pasted on pure Cu foil. A metallic lithium foil served as the counter electrode, 1 M $LiPF_6$ in ethylene carbonate (EC)-diemthyl carbonate (DMC) (1:1 in volume) was used as the electrolyte. The cells were assembled in an argon-filled glove box. The galvanostatic charge-discharge tests were performed on a land battery program-control test system (Wuhan, China) between 0.01 and 3.0 V at room temperature. The cyclic voltammetry (CV) test was carried out on an electrochemical workstation (Model 2273, Princeton Applied Research, USA) in the potential window of 0.01-3.0 V (vs. Li/Li$^+$) at a scan rate of 0.1 mVs^{-1}.
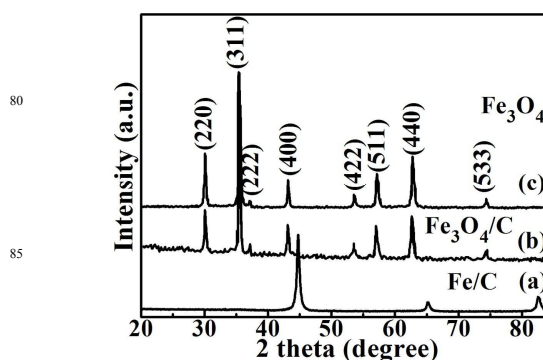
3. Results and Discussion

Fig.1 X-ray diffraction patterns of (a) sample a, (b) sample b and (c) sample c.

Fig.1 shows the XRD patterns of three samples. For sample a, three diffraction peaks can be exclusively indexed to the body-centered cubic Fe structure [JCPDS Card No: 87-0722]. For samples b and c, the XRD patterns shows that all reflections of (220),(311), (222), (400), (422), (511), (440) and (533) can be readily indexed to magnetite Fe_3O_4 [JCPDS Card No: 75-0449] with a space group of *Fd-3m*. Due to the protective carbon shell, no oxides in sample a are found, which is similar with FeNi@C, FeCo@C and Ni@C nanocapsules.[17-19] When the annealing temperature reaches 80°C, Fe nanoparticles are oxided to be Fe_3O_4, indicating a mass of defects exist in carbon shell. No peaks of other oxides such as FeO and Fe_2O_3 can be found in samples b and c, due to the fact that the annealing temperature is lower than the phase transformation temperature from the low temperature oxide of Fe_3O_4 into high temperature oxide of Fe_2O_3. It is worthy noted that the diffraction peaks of Fe_3O_4 become narrow with increasing the annealing temperature up to 200 ^{o}C, indicating the growth of Fe_3O_4 nanoparticles and complete disappearance of carbon shell. No peaks of carbon in samples a

and b are observed due to their small amount and breaking down of the periodic boundary condition in the shell structure.[14-16] Furthermore, carbon atoms usually favor to form the shell of nanoparticles in an onion-like graphite structure. The carbon shell in samples a and b will be further confirmed in the HRTEM analysis later in the paper.
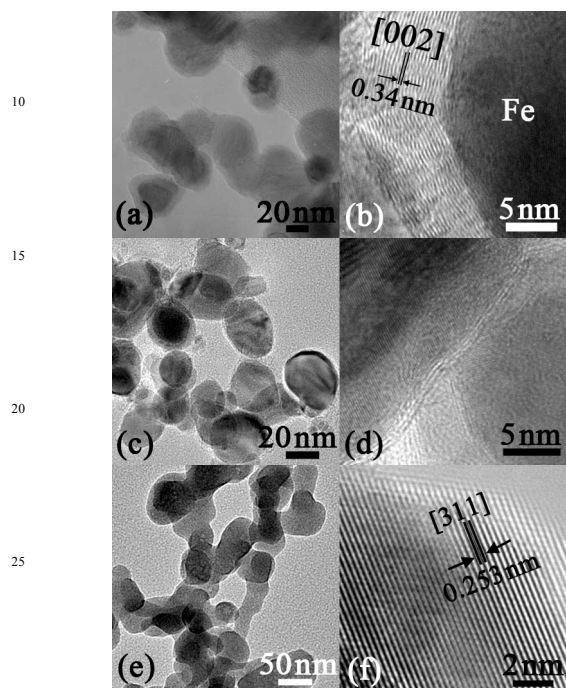

Fig.2 TEM images of (a) Fe@C nanocapsules, (c) Fe₃O₄@C nanocapsules and (e) Fe₃O₄ nanoparticles; the corresponding HRTEM images of (b) Fe@C nanocapsules, (d) Fe₃O₄@C nanocapsules and (f) Fe₃O₄ nanoparticles.

Fig.2 illustrates the morphologies and size distribution of Fe@C nanocapsules, Fe_3O_4@C nanocapsules and Fe_3O_4 nanoparticles, respectively. All these nanocapsules/nanoparticles are nearly spherical, due to the low energy principle during the nanocapsules/nanoparticles formation process.[20] As shown in Figs.2(a), 2(c) and 2(e), the size distribution of Fe@C nanocapsules, Fe_3O_4@C nanocapsules and Fe_3O_4 nanoparticles is 20-40 nm, 20-40 nm and 30-60 nm, respectively. The size of Fe_3O_4 nanoparticles is bigger than that of Fe_3O_4@C nanocapsules, which is consistent with the results of the XRD pattern. The high-resolution TEM (HRTEM) images, as shown in Figs.2(b) and 2(d), clearly indicate that Fe@C nanocapsules and Fe_3O_4@C nanocapsules own a 'core/shell' type microstructure and the inner nanoparticles are encapsulated into 'onion' type shell. The lattice plane spacing of the shell is about 0.34 nm, which corresponds to the (002) planes of a graphite phase. For Fe@C nanocapsules in Fig.2(b), the shell is above 5 nm in thickness, in which a mass of defects in the onion-like shell as a consequence of the serious bending and collapsing of the graphite atom layer. As shown in Fig.2(d), the shell of Fe_3O_4@C nanocapsules is thinner than that of Fe@C nanocapsules, indicating the defective carbon shell is slowly oxided to CO_2 gas during the annealing process. No 'core/shell' type microstructure of Fe_3O_4 nanoparticles can be observed in the HRTEM image in Fig.2(f), due to the complete

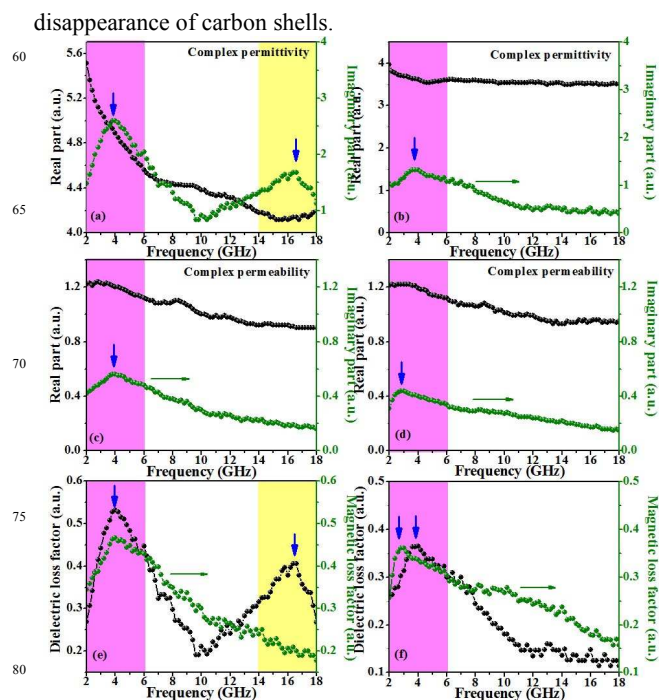disappearance of carbon shells.

Fig.3 EM parameters of Fe₃O₄@C nanocapsules (left panel) and Fe₃O₄ nanoparticles (right panel): (a, b) complex permittivity; (c, d) complex permeability; (e, f) dielectric loss factor and magnetic loss factor.

In order to investigate the intrinsic reasons for microwave absorption of Fe_3O_4@C nanocapsules, the complex permittivity (ε_γ) and permeability (μ_γ) were measured. For comparison, the microwave absorption performances of Fe_3O_4 nanoparticles were also investigated under the same conditions. Fig.3(a) shows the frequency dependence of the real part (ε') and imaginary part (ε'') of the ε_γ of the Fe_3O_4@C nanocapsules, in which exhibit two typical dielectric resonance at 4.0 and 16.6 GHz. It suggests that Fe_3O_4@C nanocapsules have strong dielectric loss against EM wave. As shown in Fig. 3(b), for the Fe_3O_4 nanoparticles, only one typical dielectric resonance can be found at 4.0 GHz. The dielectric resonance peak at 16.6 GHz may be from the effect of the onion-like carbon shell in the Fe_3O_4@C nanocapsules. In terms of the EM theory, such high dielectric loss results from the naturally physical properties of Fe_3O_4 and C and the special core/shell structures. First, the number of dipoles from the surface unsaturated atoms increases as the size decrease, resulting in an increase of the dielectric loss. Second, when the field (EM wave) was applied, electrons can transfer between Fe^{2+} and Fe^{3+} ions, which are in octahedral sites of the interstices of a face-centered cubic closed packed frame of oxygen ions. And thus, electronic spin and charge polarization have the significant effect on the loss. Third, the interfacial polarization and the associated relaxation contribute to the dielectric loss, which has been observed in the other core/shell system.[21] According to the free electron theory, $\varepsilon''=\sigma/(2\pi f\varepsilon_0)$, where σ is the electrical conductivity, the higher ε'' values of Fe_3O_4@C nanocapsules at 2-18 GHz are indicative of higher electrical conductivities, attributed to the enhancement of graphite carbon shell on the surface of Fe_3O_4 nanoparticles.[18]

Fig. 3(c) shows the μ_γ of the Fe$_3$O$_4$@C nanocapsules. It reveals that the value of the real part (μ') is in the range of 0.9-1.22. Meanwhile, the image part (μ'') first increases at 2-4 GHz, declines gradually in the 4-18 GHz. The maximum value reaches
5 0.56 at 4GHz, indicating the natural resonance. As shown in Fig.3(d), the natural resonance peak of Fe$_3$O$_4$ nanoparticles lies in 2.8 GHz. Compared with the Fe$_3$O$_4$ nanoparticles, the natural-resonance frequency of the Fe$_3$O$_4$@C nanocapsules has remarkably shifted to higher frequency, which is ascribed to the
10 considerable increase of the surface-anisotropy field (H_{eff}). H_{eff} is proportional to the effective anisotropy K_{eff} which includes the volume K_V and surface K_S contributions ($K_{eff}= K_V+6K_S/d$, where d represents the particle's size). It is well known that K_V and K_S are inversely proportional to the size of the particles.[19] Because the
15 size of Fe$_3$O$_4$ nanoparticles in Fe$_3$O$_4$@C nanocapsules is smaller than that of Fe$_3$O$_4$ nanoparticles, the larger H_{eff} in Fe$_3$O$_4$@C nanocapsules leads to the higher natural-resonance frequency. It is believed that the natural-resonance represents strong magnetic-loss abilities, implying enhanced EM-wave absorption abilities.
20 The real parts and imaginary parts of ε_γ and μ_γ correspond to the energy storage and loss of EM waves in the propagation process, respectively. The loss capacities are usually simplified by dielectric loss factor (tan $\delta_E=\varepsilon''/\varepsilon'$) and magnetic loss factor (tan $\delta_M=\mu''/\mu'$).[6] As shown in Figs. 3(e) and 3(f), the Fe$_3$O$_4$@C
25 nanocapsules exhibit both higher magnetic and dielectric loss tangents than pure Fe$_3$O$_4$ nanoparticles, implying the better microwave absorption from the Fe$_3$O$_4$@C nanocapsules in the whole frequency range of 2 to 18 GHz. Two peaks of dielectric loss factor at 4 GHz and 16.6 GHz correspond to the dielectric
30 resonance. It is worthy noted that the peaks of dielectric loss factor and magnetic loss factor in Fe$_3$O$_4$@C nanocapsules simultaneously lie in 4 GHz, meanwhile, the peak position for dielectric loss factor (4.0 GHz) and magnetic loss factor (3.0 GHz) in Fe$_3$O$_4$ nanoparticles are slightly different, which are indicative
35 of the enhanced EM wave absorption abilities from the coinstantaneous effect of dielectric loss and magnetic loss at lower gigahertz frequency range.

The microwave absorption can be further quantitatively evaluated by the value of reflection loss (RL), in which -20 dB is
40 equivalent to the 99% efficiency of microwave absorption. From the ε_γ and the μ_γ by using the Matlab procedure, the RL curves of the Fe$_3$O$_4$@C-paraffin and Fe$_3$O$_4$-paraffin composites were calculated by using the formula of transmission lines,

45 $$Z_{in} = Z_0(\mu_r / \varepsilon_r)^{1/2} \tanh[j(2\pi fd / c)(\mu_r\varepsilon_r)^{1/2}] \quad (1)$$
$$RL = 20\lg\left|(Z_{in} - Z_0)/(Z_{in} + Z_0)\right| \quad (2)$$

Where Z_0 is the free space impedance, Z_{in} the input impedance at the air-absorber interface, f the microwave
50 frequency, d the absorbent layer thickness, and c the velocity of light. In the simulation process, from the view point of the application, the absorber thickness range was set from 1.0 to 5.0 mm with an interval of 0.1 mm, in which can give the optimized condition for an absorber. The RL curves of the Fe$_3$O$_4$@C-
55 paraffin composite and Fe$_3$O$_4$-paraffin composite at various thicknesses between 2 and 18 GHz are illustrated in Figs. 4a and 4b, respectively. Fig.4(a) shows the frequency dependence of RL of the Fe$_3$O$_4$@C-paraffin composite as functions of thickness of

absorbers. For the Fe$_3$O$_4$@C-paraffin composite, RL values less
60 than -20 dB can be obtained within the 6.2-17.6 GHz frequency range by choosing an appropriate thickness of the absorbent layer from 2.4 to 5.0 mm. At the absorbent layer thickness of 3.0 mm, the absorption bandwidth of the Fe$_3$O$_4$@C-paraffin composite with RL values less than -10 dB is 7.2 GHz covering the 9.8-17.0
65 GHz frequency range. From the RL curves in Fig.4(a), it is interesting that (1) the RL peak moves to lower frequency with the increasing of the thickness; (2) the RL peak intensity first increases then decreases with the increase of the thickness when 2.0 mm < d<3.5 mm and a strong RL at 16.6 GHz can reach -45.9
70 dB when d= 2.4 mm; (3) the RL exhibits a broad peak between 9.0 and 11.4 GHz and the RL intensity can keep an approximate constant ~ -16.6 dB when d is 3.5 mm; (4) the RL peak intensity first increases then decreases with the increase of the thickness when d > 3.5 mm and a strong RL at 7.6 GHz can reach -40.6 dB
75 when d= 4.5 mm. As shown in Fig. 4(b), the RL peak of Fe$_3$O$_4$-paraffin composite intensity just increases and shifts to low frequency with the thickness. According to the EM loss model, the peaks of the dielectric loss and magnetic loss are useful to significantly absorb the EM wave energy. Hence, a strong RL
80 peak at 16.6 GHz in Fe$_3$O$_4$@C-paraffin composite may be from the dielectric loss at 16.6 GHz. As shown in Fig.3(f), the absence of dielectric loss peak at high frequency range leads to the disappearance of the strong RL peak (RL values exceeding -20 dB) in the Fe$_3$O$_4$-paraffin composite. For composites containing
85 Fe$_3$O$_4$@C nanocapsules and Fe$_3$O$_4$ nanoparticles, both the strong RL peaks are at around 7.6 GHz, which may result from the combined action of the dielectric loss and magnetic loss at low frequency range. The discrepancy between the simulated RL peaks frequency (around 7.6 GHz) and experimental dielectric-
90 magnetic loss ones (3-4 GHz) can be caused by several factors, such as the boundary condition and the modeling condition.[22] According to the EM loss model, the absorbing peak should keep at a stable frequency because the EM parameters are invariable with composite thickness. However, the simulated results show
95 that the RL peak frequency and the intensity of RL peak is closely related to the thickness. EM loss model can not be used to reasonably explain the above phenomenon. Tao et al introduced the model of an EM wave normally incident on an absorber with a backed metal plate to explain the absorbing mechanism.[23]
100 Through analyzing and calculating the energy of the EM waves reflected from the air-absorber and absorber-metal plate interfaces, it was concluded that the intensity of the RL peak is determined by the energy difference of the two waves. When the energy of the two reflected waves is equal, the intensity of the RL
105 peak is strongest; otherwise it becomes weak.[23] The quarter-wavelength cancellation condition ($d=nc/4f(\varepsilon_\gamma\mu_\gamma)^{1/2}$, (n=1,3,5…)) was proposed to well explain the phenomena.[23] Figs.4c and 4d give the dependence of λ/4 on frequency for the composites containing Fe$_3$O$_4$@C nanocapsules and Fe$_3$O$_4$ nanoparticles,
110 respectively. The vertical dot lines are extended from the RL peaks, and each line from the RL peak under an absorber thickness crosses with its corresponding thickness contour in Figs.4(c) and 4(d). The asteroid dots indicate the crossover points. All the asteroid dots are clearly observed to be on the λ/4 curve,
115 proving that all the absorber thickness are in good agreement with the quarter-wavelength of the composite when the peak appears

in the RL curve. If the *RL* peak just comes from the quarter-wavelength cancellation, *RL* value should be infinity. However, the simulated results reveal that the *RL* peak value varies with the frequency and thickness. For the above discussion, it is clearly
5 that the EM absorption mechanism can not be reasonably explained by the single EM loss model or the single quarter-wavelength cancellation condition. The combination of EM loss model and the quarter-wavelength cancellation condition can be used to explain the intensity variation and frequency of the RL
10 peak. For the different frequency range, EM loss model or the quarter-wavelength cancellation may be dominant microwave mechanism.
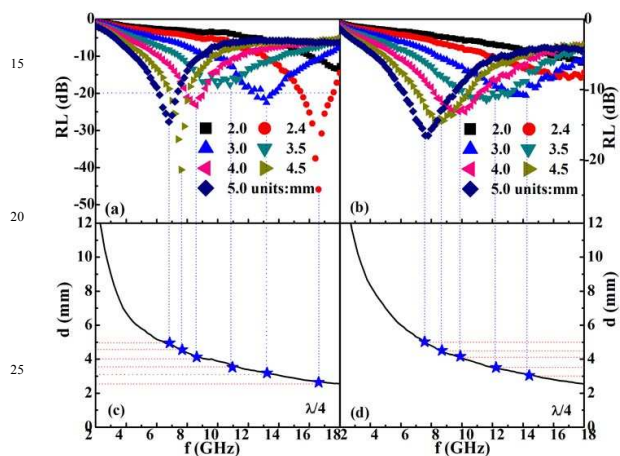

Fig.4 Frequency dependence of the *RL* of composite containing
30 40 wt.% (a) Fe_3O_4@C nanocapsules and (b) Fe_3O_4 nanoparticles, for layers of different thickness. Calculated quarter-wave principle (λ/4) maps of composite containing 40 wt.% (c) Fe_3O_4@C nanocapsules and (d) Fe_3O_4 nanoparticles.
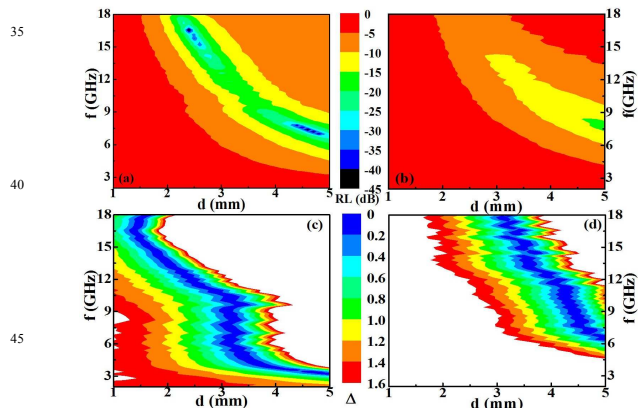

Fig.5 Calculated microwave *RL* maps of (a) Fe_3O_4@C
50 nanocapsules-paraffin composites and (b) Fe_3O_4 nanoparticles-paraffin composites. Calculated delta values maps of (c) Fe_3O_4@C nanocapsules-paraffin composites and (d) Fe_3O_4 nanoparticles-paraffin composites.

55   For the magnetic/dielectric loss absorbers, the excellent microwave absorption properties mainly results from proper EM impedance matching degree.   The EM impedance matching degree could be described as a delta-function$\Delta=\left|\sinh^2(Kfd)-M\right|$,

where *K* and *M* are determined by the relative complex
60 permittivity and complex permeability.[24] The delta value should reach zero where RL approaches minus infinity. The smaller delta value represents better EM impedance matching. According to the delta-function using the measured ε_γ and μ_γ, the calculated delta value maps of the Fe_3O_4@C-paraffin composites and Fe_3O_4-
65 paraffin composites are shown in Fig.5(c) and Fig.5(d). The dark blue area for Fe_3O_4@C-paraffin composites is obviously larger than that of Fe_3O_4-paraffin composites. Figs.5(a) and 5(b) show the obtained two-dimensional representation of *RL* derived from the Eqs. 1 and 2. The *RL* and the delta values exhibit the same
70 tendency, indicating that the enhanced microwave absorption performance of Fe_3O_4@C-paraffin composites would result from the good EM impedance matching through the core-shell microstructure.
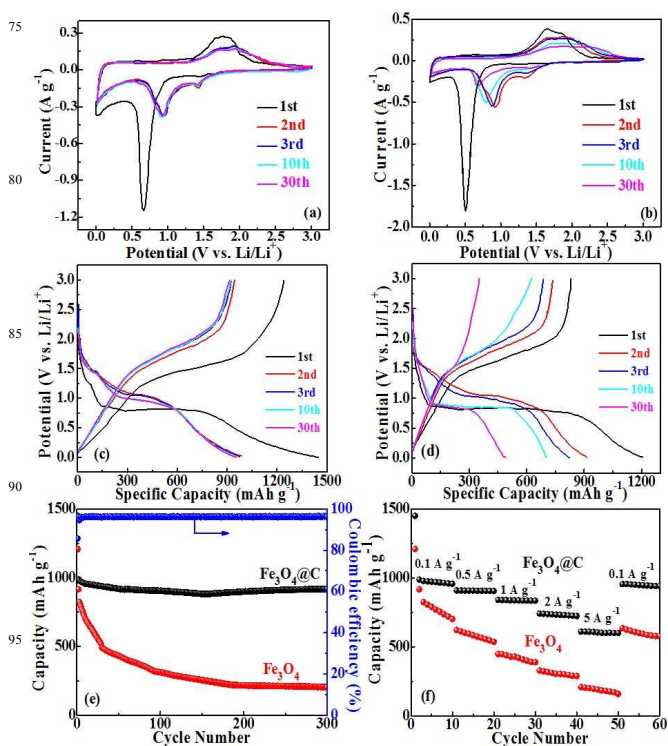

Fig.6 CV curves of (a) Fe_3O_4@C nanocapsules and (b) Fe_3O_4
100 nanoparticles electrodes for the first three cycles, 10th and 30th cycles at a scan rate of 0.1 mV s⁻¹ in the potential range of 0.01-3.0 V (versus Li/Li⁺). The charge-discharge profiles of (c) Fe_3O_4@C nanocapsules and (d) Fe_3O_4 nanoparticles electrodes
105 between 0.01 and 3.0 V at 0.1 A g⁻¹. (e) Cycle performance as a function of cycle number of the Fe_3O_4@C nanocapsules and Fe_3O_4 nanoparticles electrodes and the coulombic efficiency of Fe_3O_4@C nanocapsules in the 0.01-3 V voltage window at 0.1 A g⁻¹ for 300 cycles.(f) Multirate tests of the Fe_3O_4@C
110 nanocapsules and Fe_3O_4 nanoparticles, in order of 0.1, 0.5, 1, 2, 5 A g⁻¹, and then return to low currents of 0.1 A g⁻¹, with 10 cycles for each step.

  To evaluate the electrochemical properties of the
115 Fe_3O_4@C nanocapsules for LIB application, CV curves, galvanostatic   discharge-charge   profiles   and   cycling

measurements were conducted at room temperature in the voltage window of 0.01-3.0 V. For comparison, the electrochemical properties of Fe_3O_4 nanoparticles were also investigated under the same conditions. Figs. 6(a) and 6(b) show CV curves of $Fe_3O_4@C$ nanocapsules and Fe_3O_4 nanoparticles for the first 3 cycles, 10th cycle and 30th cycle at a scan rate of 0.1 mV s^{-1}, respectively. As can be seen, the profiles of these curves are in good agreement with the electrochemical behavior of Fe_3O_4-based anodes as described previously: $Fe_3O_4 + 8Li^+ + 8e^- \leftrightarrow 3Fe + 4Li_2O$. In the first cycle (Fig. 6(a)), the cathodic peak of $Fe_3O_4@C$ nanocapsules centered at 1.42 V corresponds to the structure transition caused by lithium insertion into Fe_3O_4 ($Fe_3O_4 + xLi^+ + xe^- \rightarrow Li_xFe_3O_4$). The sharp peak located at about 0.65 V can be attributed to the conversion of Fe_3O_4 to Fe and the formation of amorphous Li_2O ($Li_xFe_3O_4 + (8-x)Li^+ + (8-x)e^- \rightarrow 3Fe + 4Li_2O$) as well as the irreversible reaction with electrolyte. Meanwhile, the broad peak at 1.63-1.86 V is recorded in the anodic process, corresponding to the reversible oxidation of Fe^0 to Fe^{3+}. For the second cycle, both the cathodic and anodic peaks are positively shifted, which is ascribed to the structure modification of Fe_3O_4 in the first cycle and the strain introduced in Fe_3O_4 during the first cycle caused by the lithium insertion/extraction process and the polarization of the electrode materials at the first cycle.[5, 25, 26] Moreover, the CV curves of $Fe_3O_4@C$ nanocapsules in the subsequent cycles almost overlap, indicating the good cycling performance. As shown in Fig.6b, the CV curves of Fe_3O_4 nanoparticles are different from those of Fe_3O_4 nanocapsules, due to their different Li-ion insertion efficiency caused by the different sizes.[27] Nevertheless, both the peak intensity and integral areas decrease significantly during the subsequent cycles, indicating sever capacity fading.

The typical sloping voltage profiles associated with lithium alloying-dealloying with $Fe_3O_4@C$ nanocapsules and Fe_3O_4 nanoparticles can be observed in Figs.6(c) and 6(d), respectively. From Fig.6(c), it can be clearly observed that, $Fe_3O_4@C$ nanocapsules show a first discharge capacity of 1448.7 mAh g^{-1} and a charge capacity of 1240.4 mAh g^{-1} at a current density of 0.1 A g^{-1}, corresponding to a high initial coulomb efficiency of 85.6 % and Fe_3O_4 nanoparticles give a discharge capacity of 1207.9 mAh g^{-1} and charge capacity of 832.4 mAh g^{-1} in 1st cycle, with a poor columbic efficiency of 68.9 %. The extra capacity of the electrodes compared with the theoretic capacity resulted from the formation of solid electrolyte interface (SEI) film and possibly interfacial Li^+ storage during the first discharge process. The voltage hysteresis between charge and discharge could be due to the limited Li diffusion kinetics during the intercalation/deintercalation process.[28] The efficiency was increased to 95.7 % in the 2nd cycle, and above 96% after 3 cycles, indicating the formation of stable SEI layer on the surface of the carbon layer, which was favor for the cycling performance of $Fe_3O_4@C$ nanocapsules. The capacity loss is ascribed to the irreversible formation of amorphous lithium oxide and the decomposition of electrolyte and lithium salt in the formation of SEI layer, which are common for most anode materials.[29] In the subsequent cycles, the discharge capacity of $Fe_3O_4@C$ nanocapsules decreases slightly, whereas the Fe_3O_4 nanoparticles electrodes decrease markedly, indicating the $Fe_3O_4@C$ nanocapsules electrode is exceptionally electrochemical stable

during the cycling process.

Fig.6(e) presents the galvanostatic cycling curves for $Fe_3O_4@C$ nanocapsules and Fe_3O_4 nanoparticles anodes at a current density of 0.1 A g^{-1}. Apparently, $Fe_3O_4@C$ nanocapsules demonstrate a much better cyclic retention than the carbon-free Fe_3O_4 nanoparticles. After a long cycle period of 300 cycles, the reversible capacity of the $Fe_3O_4@C$ nanocapsules are able to deliver a high reversible capacity of 918 mAh g^{-1} at 0.1 A g^{-1}, which is much higher than the theoretical capacity of graphite (372 mAh g^{-1}), and its coulombic efficiency maintains consistently at ~ 96%. However, the reversible capacity of the Fe_3O_4 nanoparticles drops to 204 mAh g^{-1} at the same condition. The poor cycle life of the carbon-free Fe_3O_4 nanoparticles is ascribed to the fact that the significant volume change and the electronic accumulation of the Fe_3O_4 nanoparticles.[30]

It is noted that the capacity of $Fe_3O_4@C$ nanocapsules increases gradually during cycling after 150 cycles, which is similar with Fe_3O_4/carbon nanotubes, $Fe_2O_3@C$ and $CoO-Li_2O$ in long time cycles.[31-33] But there is so far no consensus on the reason. There are three possibilities as follows. (i) The surface area of the electrode will increase during the pulverization process, leading to more active sites for lithium storage. The pulverized particles are supposed to be still attached to the carbon shell. (ii) Fe nanoparticles generating form the initial stage will increase the overall conductivity of the electrodes, which improves the charge transfer kinetics and increases the capacity in the following cycles. (iii) Due to the decomposition of the electrolyte, organic polymeric/gel-like SEI layer is formed on the electrode surface, improving the mechanical cohesion of the active materials without hindering the ion transfer and providing excess lithium and ion storage sites, especially in the low potential region.[34] For the Fe_3O_4 nanoparticles, no increase of capacity during cycling can be observed, ascribed to the fact that no carbon shell can help the pulverized particles during cycling keep the state of aggregation.

Multiple-current galvanostatical tests were carried out to investigate the high rate performance of $Fe_3O_4@C$ nanocapsules and Fe_3O_4 nanoparticles (Fig. 6(f)). The $Fe_3O_4@C$ nanocapsules and Fe_3O_4 nanoparticles were tested at various charging/discharging rates from 0.1 to 0.5, 1, 2, 5 A g^{-1} and then regularly returned to low current rate of 0.1 A g^{-1}, with 10 cycles for each step. As observed, the capacity of Fe_3O_4 nanoparticles decrease much more quickly with the increase of current densities and cannot recover to initial levels even at low charge/discharge current after high-rate cycling. The capacity of Fe_3O_4 nanoparticles at 5 A g^{-1} is only 158 mAh g^{-1}, indicating a poor high rate performance. In contrast, the corresponding discharge capacities of $Fe_3O_4@C$ nanocapsules vary along with current densities. The reversible capacities of $Fe_3O_4@C$ nanocapsules in the last cycle at each rate were 957, 904, 834,723 and 600 mAh g^{-1},respectively, manifesting the $Fe_3O_4@C$ nanocapsules can sustain high current density without structural collapse and process excellent cycling property under high-rate testing. Finally, the discharge capacities recover to 934 mAh g^{-1} when the testing currents returned to 0.1 A g^{-1}, which was nearly same as previous measurements. The overall electrochemical performance for the core/shell structured $Fe_3O_4@C$ electrode material is superior to the previous reports of $Fe_3O_4@C$ materials.[35, 36]

Low initial coulomb efficiency and unstable cycle performance are the main obstacles for the application of high capacity Fe_3O_4@C composites. When Fe_3O_4 nanoparticles are exposed to the electrolyte, an unstable SEI and a continuous consumption of lithium can lead to the above major problems. In order to improve cycle performance of the Fe_3O_4, the composite materials with large surface areas are often designed, which inevitably results in great consumption of lithium ions in the first cycle and a low initial coulomb efficiency.[35] The Fe_3O_4 nanoparticles in our Fe_3O_4@C nanocapsules were well coated by the onion-like carbon shells. The onion-like carbon shells can accommodate volume change during the charge-discharge process. Besides, the inner defects in the onion-like carbon shell can avoid the formation of SEI on their surface, thus increasing the initial coulomb efficiency. On the base of their special core-shell structures, as-prepared Fe_3O_4@C nanocapsules show both high initial coulomb efficiency and stable cycle performance.

Conclusions

The Fe_3O_4@C nanocapsules have been synthesized by the arc discharge method and subsequently by the annealing process in air. The Fe_3O_4@C nanocapsules possess the core-shell structure, in which Fe_3O_4 nanoparticles are the cores and onion-like carbon works as the shells. HRTEM images show that a mass of defects in the onion-like shell as a consequence of the serious bending and collapsing of the graphite atom layer. The EM absorption characteristics and electrochemical performance of Fe_3O_4@C nanocapsules have been systematically investigated. Fe_3O_4@C nanocapsules exhibit two dielectric resonance at 4.0 and 16.6 GHz. Compared with Fe_3O_4 nanoparticles, the resonance at 16.6 GHz may be from the effect of the onion-like carbon shell. Due to the existence of onion-like carbon shell, the size of Fe_3O_4 nanoparticles cores in Fe_3O_4@C nanocapsules is smaller than that of Fe_3O_4 nanoparticles, which leads to the natural resonance frequency shifts to the higher frequency range. Fe_3O_4@C nanocapsules show a simultaneous enhancement of dielectric loss and magnetic loss at 2-18 GHz, which are more superior to individual Fe_3O_4 nanoparticles. At the absorbent layer thickness of 3.0 mm, the absorption bandwidth of the Fe_3O_4@C-paraffin composite with RL values less than -10 dB is 7.2 GHz covering the 9.8-17.0 GHz frequency range. An optimal RL value at 16.6 GHz can reach -45.9 dB when the matching thickness is 2.4 mm. The excellent EM absorption abilities are ascribed to the EM impedance matching and the microstructure of the Fe_3O_4@C nanocapsules. As an anode material for LIBs, the Fe_3O_4@C nanocapsules electrode show a first discharge capacity of 1448.7 mAh g^{-1} and a charge capacity of 1240.4 mAh g^{-1} at a current density of 0.1 A g^{-1}, corresponding to a high initial coulomb efficiency of 85.6 %. After a long cycle period of 300 cycles, the reversible capacity of the Fe_3O_4@C nanocapsules is able to deliver a high reversible capacity of 918 mAh g^{-1} at 0.1 A g^{-1}. The capacity of Fe_3O_4@C nanoparticles at 5 A g^{-1} is 600 mAh g^{-1}, while the discharge capacities recover to 934 mAh g^{-1} when the testing currents returned to 0.1 A g^{-1}. The remarkable electrochemical performances ascribe to the existence of onion-like carbon shell. The onion-like carbon shells not only can provide enough voids to accommodate the volume change of encapsulated Fe_3O_4 nanoparticles but also can prevent the formation of SEI films and hence the direct contact of Fe and SEI films upon lithium extraction. The enhanced EM absorption and electrochemical performances demonstrates the potential application of Fe_3O_4@C nanocapsules as effective EM absorptive anode materials for LIBs.

Acknowledgements

Notes and references

aSchool of Materials Science and Engineering, Anhui University of Technology, Maanshan,243002, China. Fax:+86 555 2311570; Tel: +86 555 2311570; E-mail: liuxianguohugh@gmail.com
bCenter for Engineering practice and Innovation Education, Anhui University of Technology, Maanshan,243032, China.
† Electronic Supplementary Information (ESI) available: See DOI: 10.1039/b000000x/

1 N.Q. Zhao, S. Wu, C.N. He, Z.Y. Wang, C.S. Shi, E.Z. Liu and J.J. Li, Carbon 2013, 57, 130-138.
2 X.Y. Zhao, D.G. Xia and K. Zheng, ACS Appl. Mater. Interfaces 2012, 4, 1350-1356.
3 Y.Z. Su, S. Li, D.Q. Wu, F. Zhang, H.W. Liang, P.G. Gao, C. Cheng and X.L. Feng, ASC Nano 2012, 6, 8349-8356.
4 H.B. Geng, Q. Zhou, Y. Pan, H.W. Gu and J.W. Zheng, Nanoscale 2014, 6, 3889-3894.
5 H. Wu, N. Du, J.Z. Wang, H. Zhang and D.R. Yang, J. Power Sources 2014, 246, 198-203.
6 X.F. Zhang, P.F. Guan and J.J. Guo, Particle &Particle Systems Characterization 2013, 30, 842-846.
7 X.F. Zhang, J.J. Guo and G.W. Qin, Appl. Phys. Lett. 2014, 104, 252404.
8 F.S. Wen, F. Zhang and H. Zheng, J. Magn. Magn. Mater. 2012, 324, 2471-2475.
9 J.H. Wang, H. Wang, J.J. Jiang, W.J. Gong, D. Li, Q. Zhang, X.G. Zhao, S. Ma, and Z.D. Zhang, Cryst. Growth Des. 2012, 12, 3499-3504.
10 J.J. Jiang, D. Li, D.Y. Geng, J. An, J. He, W. Liu and Z.D. Zhang, Nanoscale 2014, 6, 3967-3971.
11 J.Y. Gong, S.Z. Li, D.E. Zhang, X.B. Zhang, C. Liu and Z.W. Tong, Chem. Comm. 2010, 46, 3514-3516.
12 W.W. Wang and J.L. Yao, J. Phys. Chem. C 2009, 113, 3070-3075.
13 H.B. Li, W.J. Kang, B.J. Xi, Y. Yan, H.Y. Bi, Y.C. Zhu and Y.T. Qian, Carbon 2010, 48, 464-469.
14 X.G. Liu, S.W. Or, C.G. Jin, Y.H. Lv, C. Feng and Y.P. Sun, Carbon 2013, 60, 215-220.
15 X.G. Liu, S.W. Or, C.G. Jin, Y.H. Lv, W.H. Li, C. Feng, F. Xiao and Y.P. Sun, Electrochim. Acta 2013, 100, 140-146.
16 X.G. Liu, N.N. Bi, C. Feng, S.W. Or, Y.P. Sun, C.G. Jin, W.H. Li and F. Xiao, J. Alloys Compds 2014, 587, 1-5.
17 X.F. Zhang, X.L. Dong, H. Huang, Y.Y. Liu, W.N. Wang, X.G. Zhu, B. Lv and J.P. Lei, Appl. Phys. Lett. 2006, 89, 053115.
18 X.F. Zhang, X.L. Dong, H. Huang, B. Lv, J.P. Lei and C.J. Choi, J. Phys. D: Appl. Phys. 2007, 40, 5383-5387.
19 X.G. Liu, B. Li, D.Y. Geng, W.B. Cui, F. Yang, Z.G. Xie, D.J. Kang and Z.D. Zhang, Carbon 2009, 47, 470-474.
20 X.G. Liu, Z.Q. Ou, D.Y. Geng, Z. Han, Z.G. Xie and Z.D. Zhang, J. Phys. D: Appl. Phys. 2009, 42, 155004.
21 Y.J. Chen, F. Zhang, G.G. Zhao, X.Y. Fang, H.B. Jin, P. Gao, C.L. Zhu, M.S. Cao and G. Xiao, J. Phys. Chem. C 2010, 114, 9239-9244.
22 K.Y. Park, S.E. Lee, C.G. Kim and J.H. Han, Comp. Sci. Tech. 2006, 66, 576-584.
23 T. Wang, R. Han, G.G. Tan, J.Q. Wei, L. Qiao and F.S. Li, J. Appl. Phys. 2012, 112, 104903.
24 X.G. Liu, S.W. Or, S.L. Ho, C.C. Cheung, C.M. Leung, Z. Han and Z.D. Zhang, J. Alloys. Compds. 2011, 509, 9071-9075.
25 P. Wang, M.X. Gao, H.G. Pan, J.L. Zhang, C. Liang, J.H. Wang, P. Zhou and Y.F. Lu, J. Power Sources 2013, 239, 466-474.
26 L.W. Ji, Z.K. Tan, T.R. Kuykendall, S. Aloni, S.D. Xun, E. Lin, V.

Battaglia and Y.G. Zhang, Phys. Chem. Chem. Phys. 2011,13, 7170-7177.

27 Q.Q. Xiong, Y. Lu, X.L. Wang, C.D. Gu, Y.Q. Qiao and J.P. Tu, J. Alloys Compds 2012, 536, 219-225.

28 J.Q. Wang, X.L. Wang, Q.Q. Xiong, X.Y. Zhao, J.B. Cai, S. Huang, C.D. Gu and J.P. Tu, RSC Adv. 2014, 4, 322-330.

29 J.X. Guo, B. Jiang, X. Zhang and H.T. Liu, J. Power Sources 2014, 262, 15-22.

30 Y. Yu, Y.C. Zhu, JW. Liang, L. Fan and Y.T. Qiao, Electrochim. Acta 2013, 111, 809-813.

31 Y. Wu, Y. Wei, J. Wang, K. Jiang and S. Fan, Nano Lett. 2013, 13, 818-823.

32 Z. Wang, D. Luan, S. Madhavi, Y. Hu and X.W. Lou, Energy & Environmental Science 2012, 5, 5252-5256.

33 Y. Yu, C.H. Chen, J.L. Shui and S. Xie, Angewandte Chemie International Edition 2005,44,7085-7089.

34 J.S. Luo, J.L. Liu, Z.Y. Zeng, C.F. Ng, L.J. Ma, H. Zhang, J.Y. Lin, Z.X. Shen and H.J. Fan, Nano Lett. 2013, 13, 6136-6143.

35 J.Z. Chen, L. Yang, S.H. Fang and S.I. Hirano, Electrochem. Commun. 2011, 13, 848-851.

36 Z. Tan, Z.H. Sun, H.H. Wang, Q. Guo and D.S. Su, J. Mater. Chem. A 2013, 1, 9462-9468.